Analysis of the Large-Amplitude Inertia–Gravity Wave of 7 March 2008

Undergraduate Research, ATM 499 · Fall 2008–Spring 2009

JAMES H. RUPPERT JR. AND LANCE F. BOSART

Department of Atmospheric and Environmental Sciences, University at Albany, State University of New York, Albany, New York

ABSTRACT

Previous research has shown that the passage of large-amplitude inertia–gravity waves (IGWs) can have a significant impact on sensible weather. Examples of sensible weather effects associated with IGW passages include large variations in surface pressure, significant wind shifts accompanied by damaging wind gusts, and abrupt cessation of precipitation. The purpose of this analysis is to provide an overview of the environment that favors IGW genesis, organization, and maintenance, show the results of an analysis of a significant IGW event that occurred on 7 March 2008 and impacted the sensible weather over a significant part of the inland Southeast, and compare and contrast this case with previously published cases.

Surface observations and operational Doppler radar imagery displayed the signatures of large-amplitude IGW activity in the Southeast on 7 March 2008. IGW passage was accompanied by altimeter falls that exceeded 12 hPa h^{-1}, wind gusts up to 19 m s^{-1}, and a sharp back edge to the precipitation shield in radar imagery. The observed IGW activity appeared to originate in extreme southern Texas, along the Rio Grande Valley. As the IGW intensified and propagated northeastward at an estimated 30 m s^{-1}, the IGW developed a jagged wave front appearance, likely indicative of a region characterized by varying degrees of wave-ducting ability, and was most intense over parts of Mississippi and Alabama. IGW amplification occurred in a region of upper-level divergence associated with appreciable ageostrophic flow and characterized by a low-level stable layer that was situated above a surface-based layer of rain-cooled air from previous convective and stratiform precipitation.

1. Introduction

Previous research has shown that large-amplitude inertia–gravity waves (IGWs; freely-propagating gravity waves) can have significant impacts on the weather (e.g., Uccellini 1975; Lindzen and Tung 1976; Bosart and Sanders 1986; Uccellini and Koch 1987; Bosart and Seimon 1988; Ralph et al. 1993; Bosart et al. 1998). An IGW can significantly alter the amount of precipitation that accumulates at a location and its passage can be associated with damaging wind gusts. An example of how a large-amplitude IGW can affect total accumulated precipitation can be found in an analysis of a 4 January 1994 Northeast cyclone by Bosart et al. (1998). The 6-h accumulated precipitation for the period ending at 1800 UTC 4 January 1994 exhibited a very well-defined precipitation void, the western edge of which marked the eastern extent of what the authors called the "snow bomb," where rapid accumulation of snow was observed in association with cyclogenesis. It was shown by the authors that the aforementioned void was the result of the passage of a very large-amplitude IGW, associated with surface pressure falls that exceeded 13 hPa $(30\ \text{min})^{-1}$ and wind gusts up to 40 m s^{-1}. Figure 1 shows the location of the "snow bomb," the track of the large-amplitude IGW, and the accumulated precipitation for the 6-h period ending at 1800 UTC 4 January. For a more recent example, Fig. 2, showing composite WSR-88D base reflectivity for the Mid-Atlantic region at 0725 UTC 2 March 2009, reveals a knife-like back edge to the rain shield (dotted line), just northeast of a secondary region of precipitation. At 0717 UTC 2 March, surface wind gusts of 30 m s^{-1} were reported at Cape May, NJ. The latter are two readily-observable signals of the passage of the large-amplitude IGW that induced similar surface phenomena across a large swath of the Northeast and negated many total quantitative precipitation forecasts for 2 March 2009 (not shown).

The above examples of large-amplitude IGWs show the importance of gaining a better understanding of these phenomena to help improve the ability to forecast the sensible weather associated

with them. That in mind, we turn our focus to a synoptic and mesoscale analysis of the large-amplitude IGW that developed and impacted the Southeast on 7 March 2008.

This case is similar to an IGW event investigated by Bosart and Seimon (1988) that occurred on 27 February 1984, in that evaporative cooling associated with convective precipitation played a significant role in developing a surface cold pool, the boundary above which acted as a stable layer, or wave duct, about which the IGW could be maintained. A common feature to all IGWs is that their ability to propagate is governed by the presence and prominence of a wave duct. A wave duct (e.g., a temperature inversion), facilitates the propagation of an IGW by restricting its energy from dispersing vertically. A stable layer that develops in association with cold air damming, for example, is ideal for ducting large-amplitude IGWs. A detailed analysis of a case where cold air damming allows for rapid amplification and acceleration of an IGW is provided in Bosart and Seimon (1988). Another necessary criterion for wave ducts (according to Lindzen and Tung 1976) is that a critical level (CL) exist near the top of the inversion (usually well below the level of the jet). This is the level at which the wind speed and direction match that of the phase of the IGW. The CL also marks the elevation of the vertical half-wavelength, where vertical motion (ω; positive for sinking motion, negative for rising motion) ≈ 0. A detailed description of the ducted gravity wave model can be found in Lindzen and Tung (1976).

Of the IGW studies previously mentioned, none were performed recently enough to be able to take full advantage of Doppler radar data, nor have the previous investigators had access to software that is now available to facilitate advanced Doppler radar analysis (e.g., three-dimensional visualization of volume scans). With this consideration in mind, this analysis attempts to take full advantage of all new technologies available to provide a detailed synoptic and mesoscale case study of the structure and evolution of a large-amplitude IGW. Following the introduction, section 2 provides a description of the data used and methods for analysis and identifying IGW activity. Section 3 provides theoretical

background as well as a brief description of common synoptic features of IGWs. Section 4 provides a detailed analysis of observational data. Lastly, section 5 provides discussion and presents ideas for further research.

2. Data and Methodology

The University of Utah MesoWest Data Web Site (http://www.met.utah.edu/mesowest/) provided surface observations in the form of meteograms for this analysis. NWS rawinsonde data was provided in the form of skew *T*–log*p* diagrams by the University of Wyoming Atmospheric Soundings Web Site (http://weather.uwyo.edu/upperair/sounding.html). The University Corporation for Atmospheric Research Image Archive Web Site (meteorological case study selection kit; http://www.mmm.ucar.edu/imagearchive/) provided composite WSR-88D base reflectivity imagery. Various time- and cross-sectional, upper-air, and surface plots were created using the National Advanced Weather Interactive Processing System (N-AWIPS)–General Meteorological Package software and NCEP model data collected from NOAA National Operational Model Archive and Distribution System Web Site (http://nomads.ncdc.noaa.gov/). WSR–88D data collected from the National Climatic Data Center Radar Resources Web Site (http://www.ncdc.noaa.gov/oa/radar/radarresources.html) and GR2Analyst, a NEXRAD Level II display program, were employed for an analysis of the mesoscale features of the large-amplitude IGW of 7 March 2008.

For the creation of a mesoanalysis for 1200 UTC 7 March 2009 using the N-AWIPS-comprised comprehensive product generator program (NMAP2), the time-to-space conversion technique was employed. This technique was popularized in its application to mesoanalysis by Fujita in his work analyzing thunderstorms and mesoscale convective systems (e.g., Fujita 1955, Fujita 1963). In this

method, surface barograph traces (barograms) from different observing stations and from a similar time period are used to make a detailed surface mesoanalysis for one time. Though some information about the evolution of surface features is lost when extrapolating (especially in the case of very small-scale, short time-scale processes such as tornadogenesis), it provides details at a much finer spatial resolution than does an analysis using surface station data for one select time only. In this manner, one is able to put to use all of the detailed information embedded in barograms. Several other studies have employed this technique to show the fine-scale structure of IGWs (e.g., Bosart and Seimon 1988, Bosart et al. 1998).

It is necessary to specify that tracking an IGW is not a clear-cut process; there are often numerous small-amplitude (≤1 hPa) fluctuations in the surface pressure field associated with various mesoscale processes, whose magnitudes often compare to that of the main perturbation being analyzed (particularly during IGW genesis and dissipation). To track one specific IGW (or wave packet), it is necessary to synthesize all available data at hand to come up with position estimates from which IGW characteristics can be derived.

3. Background

a) Theoretical aspects of IGW behavior

Though it is extremely unlikely that IGWs are ever sinusoidal in nature (referring to the orientation of isentropes from a cross-sectional perspective), valuable information about observed IGW behavior can be gained by examining the characteristics of idealized sinusoidal-model, or theoretical IGWs. Figure 3 presents one such idealized IGW model. In imagining this theoretical IGW evolving with time, it is apparent that it is a sinusoidal propagation in which mass maxima and minima are propagating toward the right with associated upper- and lower-level divergence patterns [observed at the

surface as variations in u' (the component of the wind anomaly in the direction of wave phase)]. At columns (a) and (c), mass is converging at the surface and diverging at the CL. Ascending air parcels (maxima in $|\omega|$ exist a vertical quarter-wavelength above the surface in each column) are adiabatically cooling as the inversion height is rising (i.e., assuming realistic vertical stratification, the surface-based layer of cold air is deepening). As the columns of air adiabatically cool, p' (surface pressure anomaly; the evolution of which is associated with mass imbalances in the column) and u' increase. The opposite applies at column (b).

It can be inferred that the characteristics of the idealized ducted IGW discussed above are somewhat different from those of an observable IGW (though similarity does exist between theoretical and observable IGWs in a dry atmosphere). In reality, the background flow is nonzero. Likewise, differential advection in a vertically-sheared environment can play a significant role in altering the vertical profile of the IGW. The effects of exchanges of latent heat during phase changes of H_2O make the system substantially more complicated—an IGW can yield a release of instability and thus, a redistribution of air parcels throughout the column (as opposed to the case of the idealized ducted IGW; Uccellini 1975 has shown that an IGW of 0.5–2.5-hPa amplitude can be sufficient to alter the convective state of the atmosphere).

The manner in which the IGW-induced redistribution of air parcels often impacts the rate of precipitation is as follows: precipitation rate increases with increasing p', reaches maximum rate at maximum p' (when IGW-induced ascent has adiabatically cooled and moistened the column and increased the depth of the surface-based layer of cold air), decreases with decreasing p', and reaches minimum rate at minimum p' (when IGW-induced descent has adiabatically warmed and dried the column and decreased the depth of the surface-based layer of cold air). Oftentimes, this p'-minimum

coincides with a lasting cessation of precipitation (see previously mentioned IGW analyses for examples).

It is possible that, resultant of the fact that observable IGWs are often non-sinusoidal in nature (and often only exhibit a partial wavelength), descent-induced warming (and drying) of the column associated with decreasing p' occurs at a greater value (or over a longer duration) than ascent-induced cooling (and moistening) of the column associated with increasing p'. In order to deterministically define the mechanism for this frequently observed shutoff of precipitation with IGW passage, more investigation is necessary.

b) IGW forcing

Of 13 cases examined by Uccellini and Koch (1987) in which IGW passages had significant effects on either the rate of or total accumulated precipitation, 9 yielded common synoptic characteristics (see Uccellini and Koch 1987 for a detailed examination of the 13 cases). In most of these cases, IGW occurrence was confined to a region bounded by the upper-level inflection axis (where flow curvature changes from cyclonic to anticyclonic), the jet axis, the ridge axis, and the surface frontal boundary. Figure 4 presents a schematic representation of this synoptic environment. It is no surprise that IGW occurrence is commonly on the cold side of the surface frontal boundary, for it is in this region where a frontal inversion (i.e., a wave duct) is often located. In cases where the IGW propagates on the warm side of a surface frontal boundary (as in the case analyzed by Bosart and Seimon 1988), evaporative cooling (from falling precipitation) and the development of a surface-based cold pool to stabilize the boundary layer leads to the formation of low-level wave ducts.

The scenario that has been presented above is not a rare occurrence—wave ducts exist with many frontal systems and can develop via many other processes that are not discussed here. What is

necessary in conjunction with a wave duct is a perturbation to initiate IGW propagation. Likewise, to prevent IGW dissipation, the wave duct must be sufficiently strong and exist in conjunction with a CL (to meet the necessary criteria for a ducted gravity wave, as defined by Lindzen and Tung 1976). Means for perturbation of the wave duct can be deep convection, mesoscale ascent ahead of a vigorous trough, or vigorous vertical motions accompanying unbalanced ageostrophic flow.

One scenario in which significant unbalanced flow can develop in the upper troposphere is when the half-wavelength between the trough axis and the downstream ridge axis decreases, under the assumption of gradient wind balance (GWB). This balance is governed by

$$\frac{V^2}{\pm R}-\frac{1}{\rho}\left|\frac{\partial p}{\partial n}\right|+\left|f\right|V=0, \tag{1}$$

where V is the total wind, R is the radius of flow curvature (positive for cyclonic flow, negative for anticyclonic flow), ρ is density, p is pressure, n is the unit vector $\perp$ to the left of flow direction, and f is the Coriolis parameter. Considering the sign of R and assuming equality of the pressure gradient (and thus, of the geostrophic wind) throughout an idealized, sinusoidal Rossby wave-train, rearrangement of Eq. (1) allows one to infer that for flow within a trough,

$$V<V_g, \tag{2}$$

or wind is subgeostrophic. Here, V_g represents the geostrophic wind:

$$V_g=\frac{1}{\rho\left|f\right|}\left|\frac{\partial p}{\partial n}\right|. \tag{3}$$

It can also be inferred that for flow within a ridge,

$$V>V_g, \tag{4}$$

or wind is supergeostrophic. Once can also infer that the smaller R is (i.e., the more curvature the flow exhibits), the more the flow deviates from geostrophy. Thus, in this idealized wave-train, air parcels

must accelerate from subgeostrophic to supergeostrophic as they exit the base of a trough and enter the crest of a downstream ridge. It can be inferred that, in a highly-amplified pattern [e.g., R<500 km (5×10^5 m)], these accelerations could yield significant quantities of divergence (>14×10^{-5} s^{-1} in the case of 7 March 2008). The vertical motions associated with this upper-level divergence can potentially be vigorous enough to initiate or amplify an IGW (assuming a wave duct is present), as is believed to be the case for 7 March 2008.

Another process that has been cited as a mechanism for the formation of large-amplitude IGWs is related to mesoscale phenomena. Pressure gradients between wake lows (aka mesolows) and mesohighs (aka "bubble" highs) associated with convective squall lines (CSLs) have been observed in excess of 5 hPa $(20\ km)^{-1}$ (e.g., Johnson 2001). A pressure gradient of this magnitude is similar to that which would be expected across the front of a large-amplitude IGW. Wake lows (normally found at the back edge of the trailing stratiform precipitation region behind a CSL) have occasionally been observed to "break off" from the convection, usually accelerating ahead of the CSL as an IGW (as in the case investigated by Bosart and Seimon 1988). The processes by which (or how often) this "break" occurs as well as distinguishing features between wake lows and IGWs currently remain elusive, though further investigation (e.g., modeling and climatological analyses) would likely reveal vital information for a better understanding of the phenomena addressed here.

3. Synopsis

Figure 5 presents a continuity map showing two-hourly isochrones of the large-amplitude IGW of 7 March 2008 as well as key stations to be reference throughout this analysis. Around 0200 UTC 7 March 2008 (herein, simply 02Z/7), small variations (<1 hPa) in analyzed station altimeter values begin to appear near the Rio Grande Valley in southern TX (herein, analyzed station altimeter is referred to as

surface pressure). From 02–06Z/7, the IGW intensifies very little as it propagates northeastward at an estimated phase speed of 30 m s^{-1}. Subsequent to 06Z/7, the IGW is observed to intensify, reaching maximum amplitude (12 hPa) near the MS–AL border around 11Z/7. It is around this time that the IGW decelerates to an estimated 25 m s^{-1}, as the wave front begins to develop a jagged shape. This deceleration and wave-front deformation may be related to the IGW's propagation into a region characterized by varying degrees of ducting ability, but further investigation is necessary (and ongoing) to qualify this hypothesis. Subsequent to 12Z/7, the IGW is observed to weaken, becoming virtually indiscernible in the surface pressure field beyond 18Z/7.

a) Synoptic overview

Figure 6 presents maps of 300-hPa height and wind derived from the half-degree NCEP–GFS analyses for 00, 06, 12, and 18Z/7. At 00Z/7, there is a trough (long dash–dotted line) that extends south, well into Mexico. A short-wave ridge (dotted line) is located just downstream of the trough axis, in between two jet streaks (with winds >60 m s^{-1}), and more specifically, in overlapping regions of implied jet streak-induced upper-level divergence (poleward exit region of southernmost jet streak and equatorward entrance region of northernmost jet streak). Important to note is that subsequent to 12Z/7, the half-wavelength between the trough and downstream ridge lengthens significantly with time. Considering this observed increase in downstream half-wavelength and ignoring temporal changes in the magnitude of the height gradient between the trough and downstream ridge, one can infer (through a GWB perspective) that air parcel accelerations from the base of the trough to the crest of the ridge (and thus, a potential IGW amplification mechanism) are (is) decreasing during this 12-h time period. Also important to note is that, though IGW genesis occurs between the trough and inflection axes [it is hypothesized that genesis occurs near the Rio Grande Valley; assuming that the height field is similar

during genesis to what is represented in Fig. 6 (a)], the IGW remains situated between the inflection and ridge axes for the remainder of its observed lifetime [i.e., within the IGW occurrence region shown in Fig. 4 (with respect to upper-level features)].

Maps of sea level pressure (SLP), 1000–500-hPa thickness, and 10-m wind derived from the 20-km NCEP–RUC analyses for 00, 06, 12, and 18Z/7 show the southeastward progression of cold air across the Southeast and Gulf of Mexico during this period (Fig. 7). In noting that by 00Z/7, the leading edge of the cold air is at the southernmost extent of TX and protruding into central-northern Mexico, it can be inferred that a layer of cold air is in place at the surface in this region at the time of IGW genesis (believed to occur near 02Z/7). This is especially the case in the Rio Grande Valley, where dense, cold air seeps down sooner than it reaches the higher surrounding elevations. Likewise, note that the IGW remains in the cold air throughout its subsequent lifetime. This confirms that the IGW occurrence region for the case of 7 March 2008 is consistent with the cases analyzed in Uccellini and Koch (1987; as shown in Fig. 4).

b) Genesis

A meteogram for Hebbronville (HBV), TX for the 24-h period ending at 22Z/7 reveals a surface pressure perturbation near 02Z/7 that is comparable in magnitude to numerous other surface pressure perturbations (Fig. 8). Unique to this surface pressure perturbation, however, is that it is coincident with a temporary veering of the wind toward north-northeasterly. This temporary shift in wind direction, though slight, is consistent with the passage of a low-level divergence zone followed closely by a convergence zone associated with an IGW. The latter compares to the passage a half-wavelength of the idealized ducted gravity wave from Fig. 3 [from column (a) to column (b)], suggesting that a wave of

depression (one that induces surface pressure falls followed by surface pressure rises) has propagated through HBV.

A sounding for Corpus Christi (CRP), TX at 00Z/7 confirms the presence of a wave duct in this region by revealing a shallow layer of cold air, capped by a frontal inversion from 950–900 hPa (Fig. 9). Despite the presence of an inversion, not all of the necessary criteria for a ducted gravity wave (as defined by Lindzen and Tung 1976) are met—note the lack of a CL near the top of the inversion [IGW phase speed at 02Z/7 is approximately 30 m s^{-1} (58 kt) while, based on Fig. 9, a 30-m s^{-1} wind speed is not observed below 400 hPa]. It can be inferred that, if the necessary criteria for a ducted gravity wave are in fact met, a CL develops between 00Z/7 and the time that the IGW propagates through this region. Clarification of whether or not a CL is indeed present at the time of IGW passage at HBV (or at the time of genesis) is a goal of ongoing research (20-km NCEP–RUC model analysis data is being utilized to "fill in the gaps," both spatially and temporally).

No radar signatures exist with IGW passage at this location (nor at any west of LA) because there was no precipitation at the time. This is confirmation that IGW genesis was not related to the "breaking off" of a wake low from a CSL near the TX–Mexico border. Though it is hypothesized that terrain-airflow interactions over eastern Mexico may have played a role in initiating the originally small-amplitude IGW, only preliminary investigation has been done to find certainty in this.

c) Amplification

Examination of composite WSR-88D base reflectivity for the regions of the southern and northern Mississippi River Valley at 00, 06, 12, and 18Z/7 reveals the progression of a large swath of convective and stratiform precipitation across the Gulf region (Fig. 10). This precipitation swath is associated with significant accumulations across southern MS [e.g., 24 mm at Hattiesburg-Laurel

Regional Airport (PIB), MS]. A vertical time section for Jackson Thompson Field (JAN), MS derived from NCEP–RUC analyses for 00–12Z/7 reveals the thermodynamic evolution associated with the passage of this precipitation (Fig. 11). Note the decrease in potential temperature of 10 K and increase in relative humidity from <50 % to >90 % near the surface, all within a 4-h period (from 05–09Z/7). Soundings for JAN at 00 and 12Z/7 show the observed enhancement of a stable layer that, by 12Z/7, extends from 950–750 hPa (this enhancement is also exhibited by the increase in vertical stratification of potential temperature in Fig. 11 during this 12-h period; Fig. 12). An inference can be made that, though radiative cooling and cold air advection likely aided to the decrease in surface temperature between 00 and 12Z/7 at JAN, appreciable low-level evaporative cooling played the key role in the strengthening of the wave duct in this region.

WSR-88D base reflectivity and velocity for Jackson (DGX), MS at approximately 08Z/7 (0802 UTC) reveals inbound velocities of 33 m s^{-1} (approximately = IGW phase speed) on a sharp back edge of the reflectivity and collocated with the IGW (Fig. 13). These inbound velocities were observed at approximately 800 hPa (1540 m AGL), or roughly 50 hPa below the top of the inversion (assuming that the vertical profile is similar that observed at JAN at 12Z/7). Likewise, a similar wind speed is exhibited in Fig. 12 (b; though roughly 200 hPa above the top of the inversion). Note also that the direction of this wind observation is similar to the direction of IGW propagation (approximately southwesterly). It can be inferred that the aforementioned observations represent a CL.

Between 06 and 12Z/7, the IGW is observed to propagate in the wake of the precipitation and along a stable layer similar to that which was just discussed (one enhanced by evaporative cooling). Not so similar though, is the intensity with which the IGW propagates subsequent to 06Z/7, as surface pressure perturbations associated with IGW passage are observed to increase by 9 hPa within 6 h. A meteogram for Jasper (JAS), TX for the time period encompassing wave passage (approximately 06Z/7)

shows a drop in surface pressure of 3 hPa, corresponding with a temporary veering of wind to east-northeasterly and an increase in gusts of 2 m s^{-1} (Fig. 14). A meteogram for the same time period for JAN shows a drop in surface pressure of 10 hPa with associated wind gusts up to 18 m s^{-1} from the northeast (Fig. 15). It is evident that Figs. 14 and 15 exhibit the passage of a wave of depression, as did the meteogram for HBV (cf. Fig. 8).

It is likely that the observed IGW amplification between 06 and 09Z/7 is, at least in part resulting from the aforementioned enhancement of the wave duct by evaporative cooling, though around the time of wave amplification, the IGW is observed to be collocated with a region of significant upper-level divergence associated with appreciable ageostrophic flow. This collocation is shown in maps of 300-hPa height, ageostrophic wind, divergence, and total wind derived from 20-km NCEP–RUC analyses for 06 and 10Z/7 (Fig. 16). At 06Z/7, note the region of significant northwesterly ageostrophic flow in extreme southeastern TX (likely associated with the deceleration of air parcels exiting the southernmost jet streak), as well as the extensive region (including parts of TX, LA, OK, AR, KS, and MO) of significant easterly and south-easterly ageostrophic flow along the northern TX–LA border and north (likely associated with the acceleration of air parcels entering the northernmost jet streak). Also note the component of the ageostrophic wind approximately parallel to the 300-hPa height contours (related to GWB) at 06Z/7. It is likely that upper-tropospheric accelerations resultant from highly-curved flow (GWB perspective) as well as from jet streak-induced secondary circulations are working in sync to induce of significant quantities of divergence, in some regions exceeding 14×10^{-5} s^{-1}. It is hypothesized, but has yet to be determined with certainty, that the region of upper-level divergence (and implied vigorous vertical motion associated with it) collocated with the IGW at 06Z/7 contributes significantly to the observed IGW amplification. Note also that at 10Z/7, the IGW maintains collocation with a maximum in upper-level divergence. More specifically, this collocation is in the region where the IGW

is observed to exhibit its greatest amplitude (central MS). A meteogram for Columbus Air Force Base (CBM), MS for the time period encompassing wave passage (approximately 11Z/7) shows a drop in surface pressure of 12 hPa over a 1-h span (Fig. 17). This rapid decrease in surface pressure corresponds with a veering of the wind from northerly to northeasterly with gusts up to 19 m s^{-1}.

Presented in Fig. 18 is a manually-generated surface analysis for 12Z/7 (1 h after IGW passage at CBM), showing SLP, composite WSR-88D base reflectivity, and the IGW. It can be inferred from this figure that the IGW-induced vertical motions are yielding a redistribution of moisture throughout the column, such that the column dries enough for the precipitation to cease with IGW passage (despite lingering base reflectivity in the wake of the IGW near extreme northwestern AL). Most important to note in Fig. 18 is the pronounced SLP minimum (<1002 hPa) along the indicated position of the IGW (dotted line). Also note the intense horizontal pressure gradient [and its asymmetry; approximately 10 hPa $(25\ km)^{-1}$] about the IGW, consistent with time-to-space conversion methods. It can be inferred that this pressure gradient is the cause of the wind shifts and high gusts observed at the aforementioned surface stations.

It is unquestionable that the winds observed within this strong pressure gradient ($\leq$19 m s^{-1}) are subgeostrophic, which would otherwise be on the order of 200 m s^{-1}! The two reasons (as discussed in Johnson 2001) that the observed winds are lower than one might expect, considering the magnitude of the pressure gradient, are that friction restricts the wind accelerations, preventing them from even coming close to reaching geostrophy (only considering magnitude), and that the durations of the accelerations are only as long as IGW-induced pressure gradients are present at one location for (roughly 0.5–1 h).

Though it is likely that the IGW has undergone some degree of evolution between the time of passage through CBM and 12Z/7, one can still observe that the altimeter trace presented in Fig. 17

compares quite well to the SLP analysis presented in Fig. 18. For example, note the slight rise in surface pressure just prior to the unmistakable crash at CBM and compare that to the ridge ahead of the IGW in Fig. 18 (though at 12Z/7, the ridge appears to be spread over a larger region than is evident in Fig. 17).

d) Dissipation

Figure 19 presents a sounding for Nashville (BNA), TN at 12Z/7. Compared to the 200-hPa thick inversion observed at JAN [see Fig. 12 (b)], it can be inferred that the stability exhibited by the BNA sounding might not be characteristic of a wave duct sufficient to contain the IGW associated with 12-hPa surface pressure perturbations (as observed at CBM). Following passage through TN, a small drop in surface pressure (2 hPa) can be seen near 18Z/7 in a meteogram for Wilmington (ILN), OH (Fig 20). Subsequent to wave passage at ILN, and although the IGW is still within the cold air and in the wake of the precipitation, it dissipates beyond recognition in the surface observational data (satellite data suggests the possibility of a lasting IGW, beyond 18Z/7, but confirmation is pending).

A feature worth noting in Fig. 18 is the secondary trough that extends from northwestern GA, northeast along the western flank of the Appalachian Mountains (along the TN–NC border). Though the data is to partially obscured (or perhaps, too lacking in spatial resolution), one can note several stations showing east and southeasterly winds along the east side of this trough. These wind observations together with the presence of the synoptic-scale trough suggest that downsloping and surface warming may be occurring to the lee (western side in this case) of the Appalachians.

Figure 21 presents a map of 850-hPa height, wind, temperature, and thermal advection derived from 20-km NCEP–RUC analysis data for 12Z/7. The wind pattern about the Appalachians shown in this figure (largely south-southeasterly flow) reaffirms what was previously posited, that downsloping may be occurring to the lee of the mountains. If sinking motion is occurring lee of mountains, this, in

theory, might be leading to a vertical expansion of the boundary layer and thus, a weakening and/or a mixing out of the low-level inversion (i.e., breaking down of the wave duct necessary for IGW maintenance). More corroboration is necessary before this can be conclusive, but it is hypothesized that downsloping plays a significant role in the dissipation of the IGW between 12 and 18Z/7.

4. Concluding Remarks

The passage of a large-amplitude IGW on 7 March 2008 was, in its most intense state, associated with surface pressure falls of 12 hPa $(1\ h)^{-1}$, surface wind gusts of 19 m s^{-1}, and an abrupt ending to the precipitation. It is hypothesized that the IGW originated near the Rio Grand Valley and was the result of the perturbation of a wave duct (low-level frontal inversion) by terrain–airflow interactions in eastern Mexico. Throughout its lifetime (subsequent to genesis), the IGW remained within the cold air and between an upper-level short-wavelength ridge axis and upstream inflection axis (i.e., within the IGW occurrence region shown in Fig. 4). It intensified in a region characterized by significant 300-hPa divergence associated with appreciable ageostrophic flow [likely related to jet streak-induced secondary circulations as well as a strongly-curved flow pattern] and along a low-level wave duct that was enhanced by low-level evaporative cooling. Dissipation was observed in a region of potential downslope flow on the western flank of the Appalachian Mountains (which might have served to weaken or destroy the wave duct).

As mentioned previously, more investigation is necessary to tie down loose ends with regards to IGW genesis, maintenance, amplification, and dissipation mechanisms. All of the hypotheses mentioned will be investigated in order to refute or secure them into the knowledge of IGWs. This is very relevant to weather forecasting since after all, IGWs have been shown to cause significant mischief at the surface. What has not been shown, though what could almost certainly be proven with ease is the threat that the phenomena pose toward aviation. The authors leave this for another analysis.

Acknowledgements. This research would not have been possible without the help of many of the students and faculty members at the Department of Atmospheric and Environmental Sciences (DAES) at the University at Albany, State University of New York, in providing computer programming assistance as well as intellectual advice. I particularly thank Dr. Lance Bosart (DAES Distinguished Professor) who provided invaluable advice, both for the direction of this research project and for the direction of intellectual growth and development for an aspiring scientist. I would like to extend special thanks to Kevin Tyle (DAES Systems Administrator), Ross Lazear (DAES Instructional Support Specialist), and DAES graduate students Heather Archambault, Jonas Asuma, Jason Cordeira, Thomas Galarneau, Nicholas Metz, Brian Silviotti, and Alan Srock for assistance, both in computing and in preparation for presentations of this work. I would like to thank Darren Van Cleave (graduate student at the Department of Atmospheric Science at Colorado State University) for providing online satellite data resources. I would like to thank Steven Koch (NOAA/Earth System Research Laboratory) for advice on numerical analysis for this work. I extend great thanks to Anton Seimon (Wildlife Conservation Society, Bronx, NY) and Michael Landin (former DAES staff member) for instructional as well as motivational discussion of IGWs. Lastly, I extend thanks to all those who contributed to both motivational and intellectual discussions of IGWs via the DAES research (map) email list.

References

Bosart, L. F., and F. Sanders, 1986: Mesoscale structure in the megalopolitan snowstorm of 11–12 February 1983. Part III: A large-amplitude gravity wave. *J. Atmos. Sci.*, **43**, 924–939.

——, and A. Seimon, 1988: A case study of an unusually intense atmospheric gravity wave. *Mon. Wea. Rev.,* **116,** 1857–1886.

——, W. E. Bracken, and A. Seimon, 1998: A study of cyclone mesoscale structure with emphasis on a large-amplitude inertia–gravity wave. *Mon. Wea. Rev.,* **126,** 1497–1527.

Fujita, T. T., 1955: Results of detailed synoptic studies of squall lines. *Tellus,* **7,** 405–436.

——, 1963: Analytical mesometeorology: A review. *Severe Local Storms, Meteor. Monogr.,* No. 27, Amer. Meteor. Soc., 77–125.

Johnson, R.H., 2001: Surface mesohighs and mesolows**.** *Bull. Amer. Meteor. Soc.*, **82,** 13–31.

Lindzen, R. S., and K. K. Tung, 1976: Banded convective activity and ducted gravity waves. *Mon. Wea. Rev.,* **104,** 1602–1617.

Ralph, F., V. Venkateswaran, and M. Crochet, 1993: Observations of a mesoscale ducted gravity wave. *J. Atmos. Sci.*, **50**, 3277–3291.

Uccellini, L. W., 1975: A case study of apparent gravity wave initiation of severe convective storms. *Mon. Wea. Rev.,* **103,** 497–513.

——, and S.E. Koch, 1987: The synoptic setting and possible energy sources for mesoscale wave disturbances. *Mon. Wea. Rev.*, **115**, 721–729.

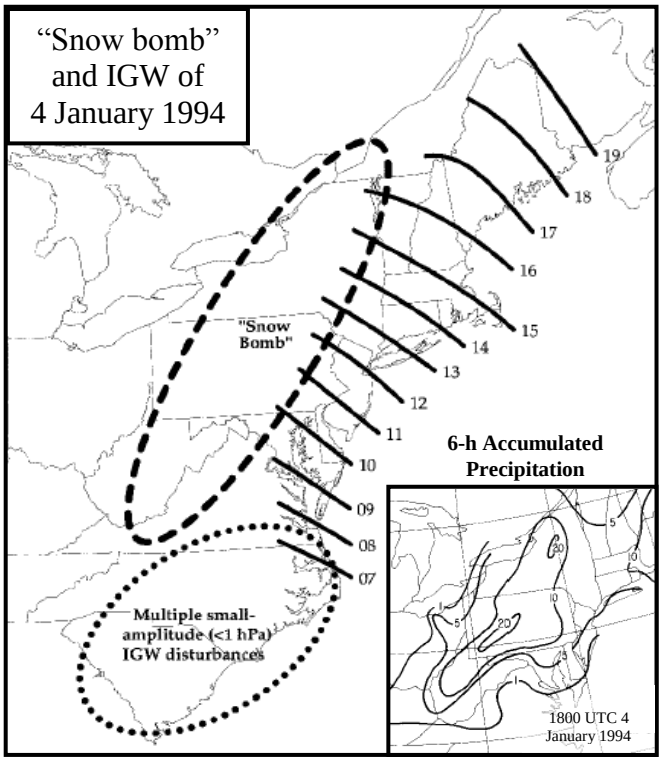

FIG. 1. Large-amplitude inertia–gravity wave (IGW) isochrone analysis for 0700–1900 UTC 4 January 1994. Locations of "snow bomb" and region characterized by multiple small-amplitude (<1 hPa) IGW disturbances are indicated. Inset shows accumulated precipitation (contoured for 1, 5, 10, and 20 mm) for the 6-h period ending at 1800 UTC 4 January 1994. From Figs. 1 and 10 (c) of Bosart et al. (1998), respectively.

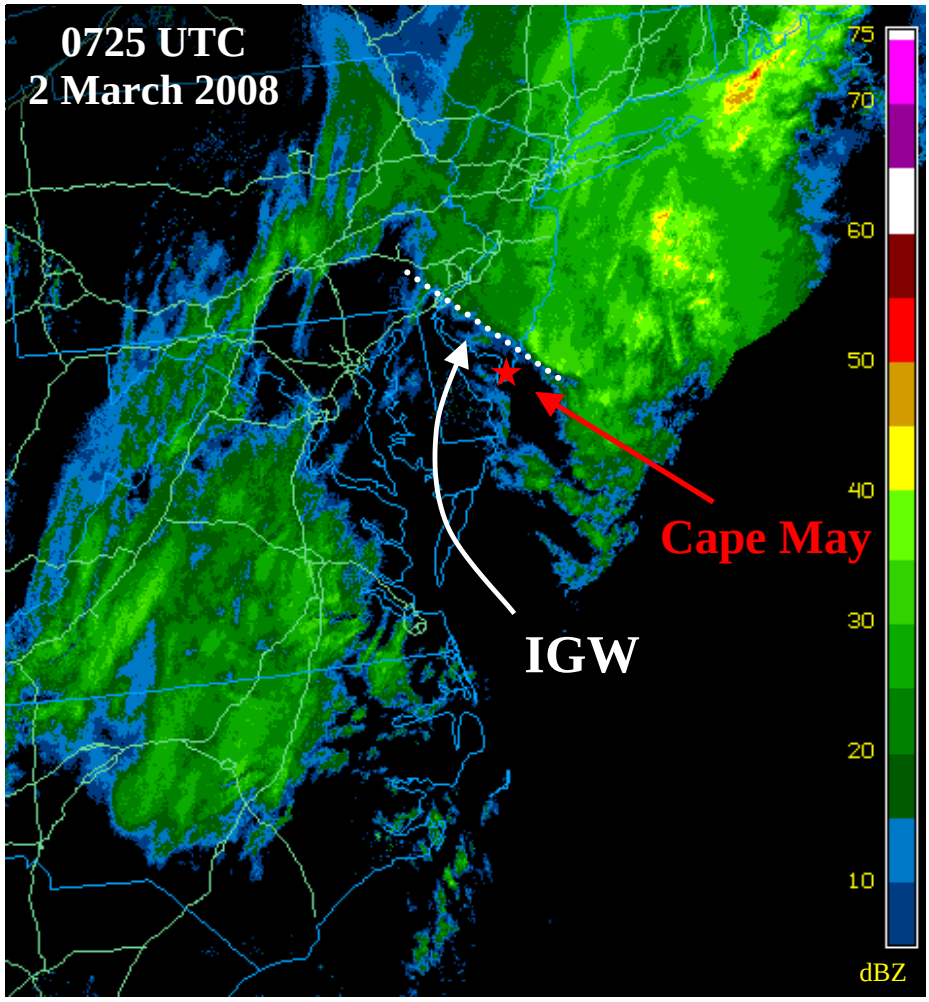

FIG. 2. Composite WSR-88D base reflectivity for the East Coast at 0725 UTC 2 March 2009. Locations of IGW and Cape May, NJ are indicated. From the University Corporation for Atmospheric Research (UCAR) Image Archive (http://www.mmm.ucar.edu/imagearchive/).

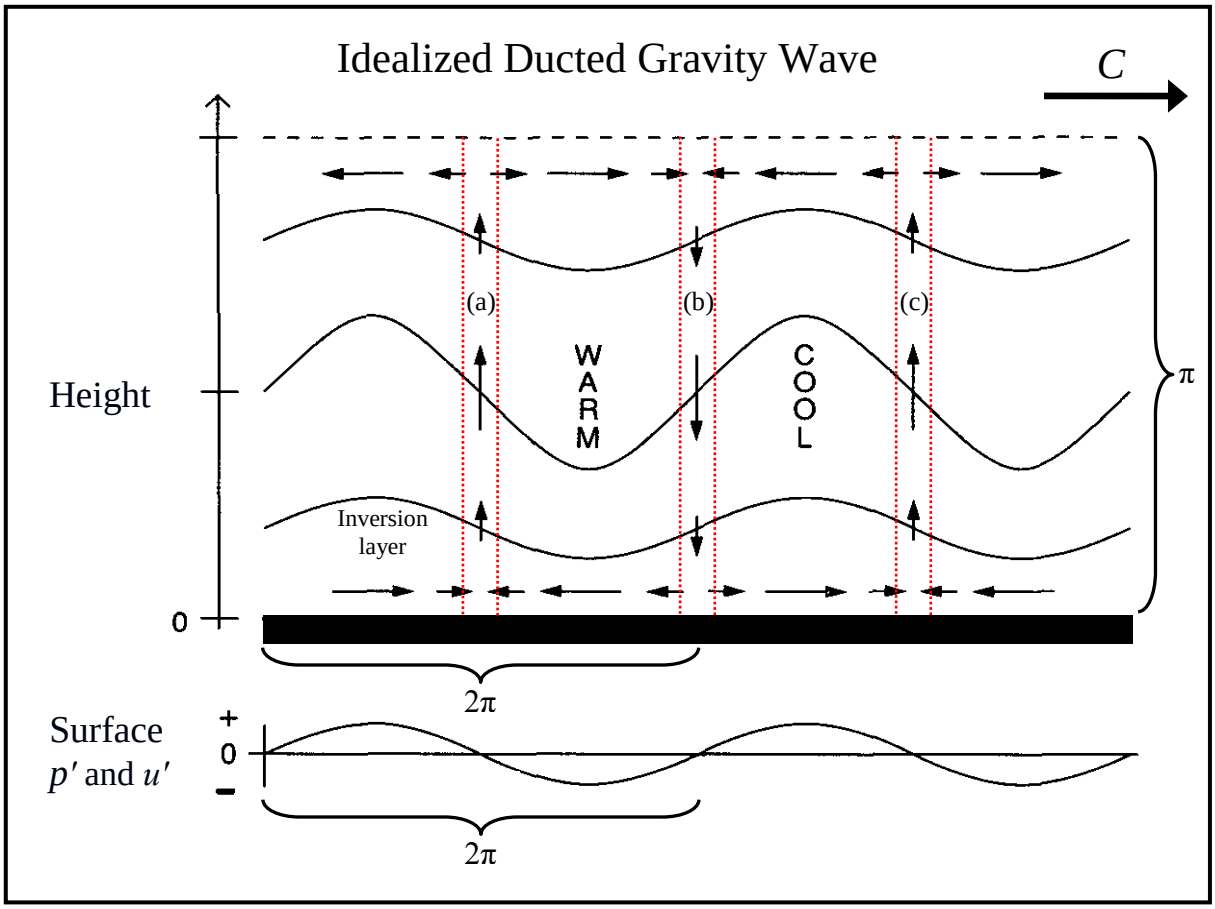

FIG. 3. Schematic representation of an idealized ducted gravity wave propagating within a dry atmosphere with no background flow and, for simplicity, no Coriolis force. Phase (C) direction is to the right, as indicated by the heavy arrow. Top graph is a vertical cross section perpendicular to wave phase showing the critical level (CL; dashed line), isentropes (solid lines), the surface (shaded), and wave-induced horizontal and vertical motions (thin arrows, where length $\propto$ magnitude). Inversion layer and temperature anomalies associated with wave-induced vertical parcel displacements are indicated. Bottom graph shows wave-induced surface pressure and u-wind anomaly (v-wind = 0; p' and u', respectively) across the same horizontal section, where u' represents the component of the wind wave phase (positive to the right). The horizontal full- and vertical half-wavelengths are indicated. Note the locations of columns a, b, and c (regions enclosed by dotted lines, whose locations are fixed relative to the surface). Modified from Fig. 15 of Ralph et al. (1993).

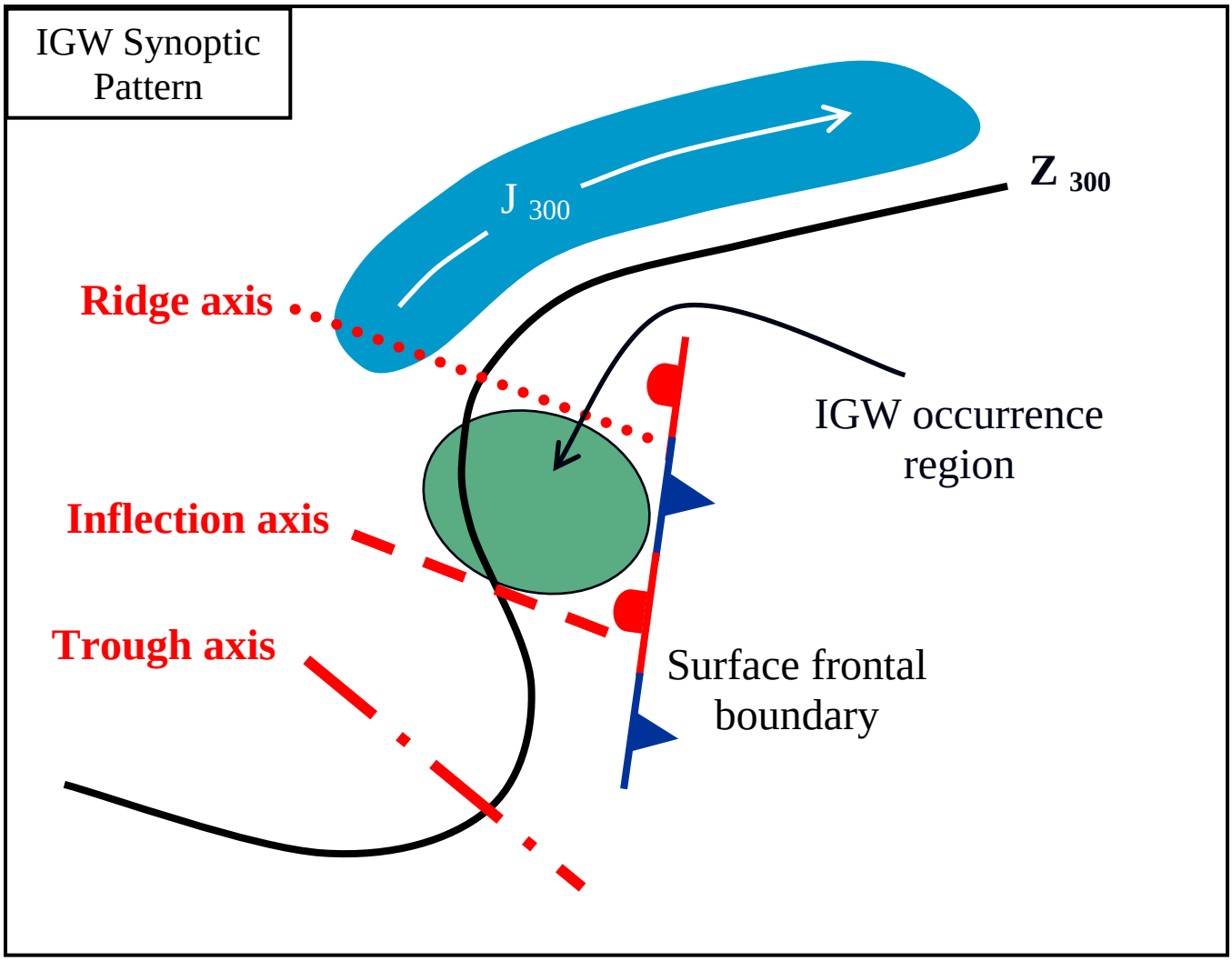

FIG. 4. Schematic representation of the synoptic pattern common to most large-amplitude IGW events. Locations of IGW occurrence region, surface frontal boundary, and 300-hPa jet streak (shaded in blue for values >40 m s^{-1}), height contour (thick solid line; 912 dam), and ridge, inflection, and trough axes are indicated. Modified from Fig. 1 of Uccellini and Koch (1987).

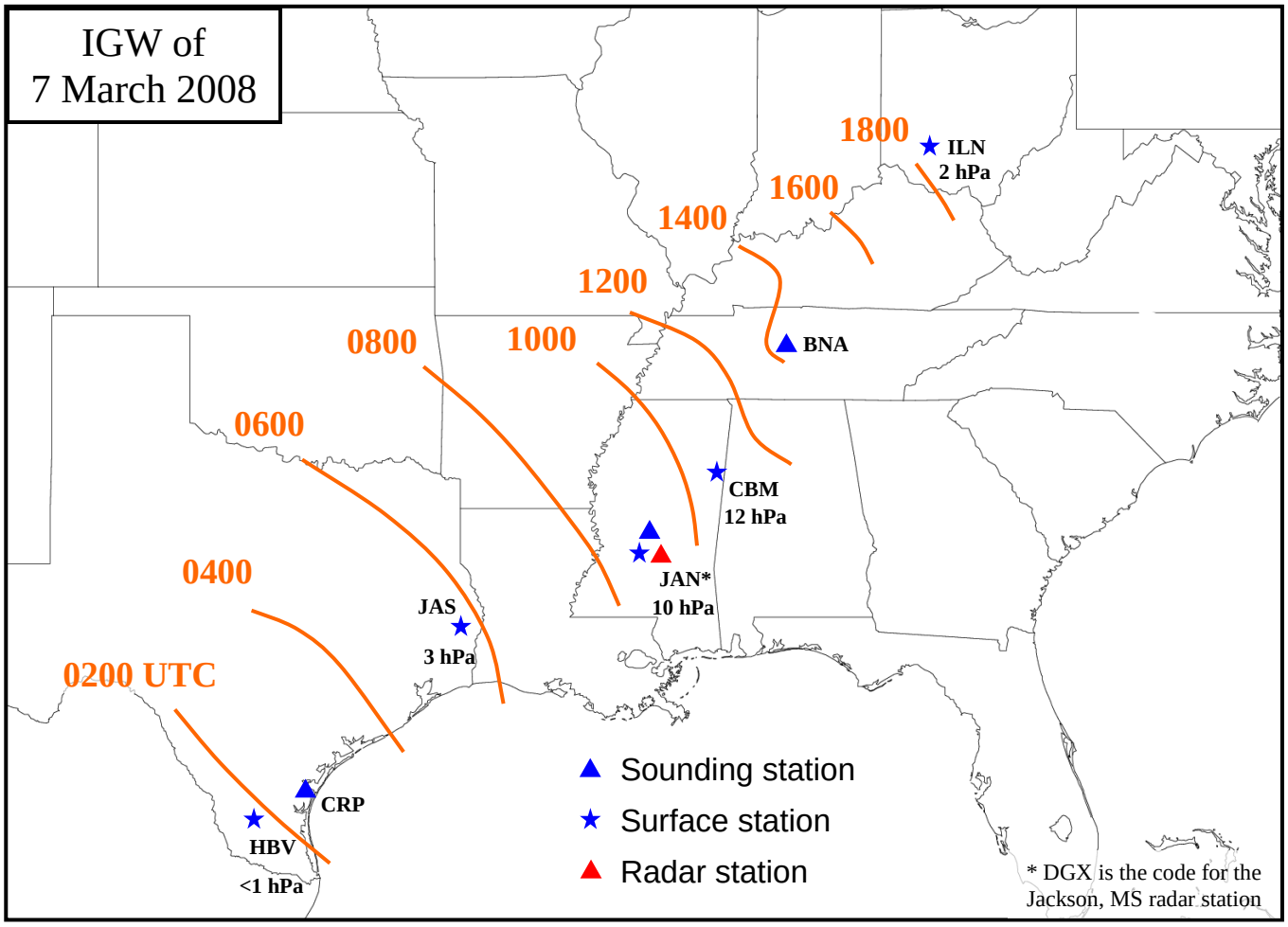

FIG. 5. Large-amplitude IGW isochrone analysis for 0200–1800 UTC 7 March 2008. Locations of key stations for this analysis are indicated. IGW-induced surface altimeter perturbation is noted below each surface station.

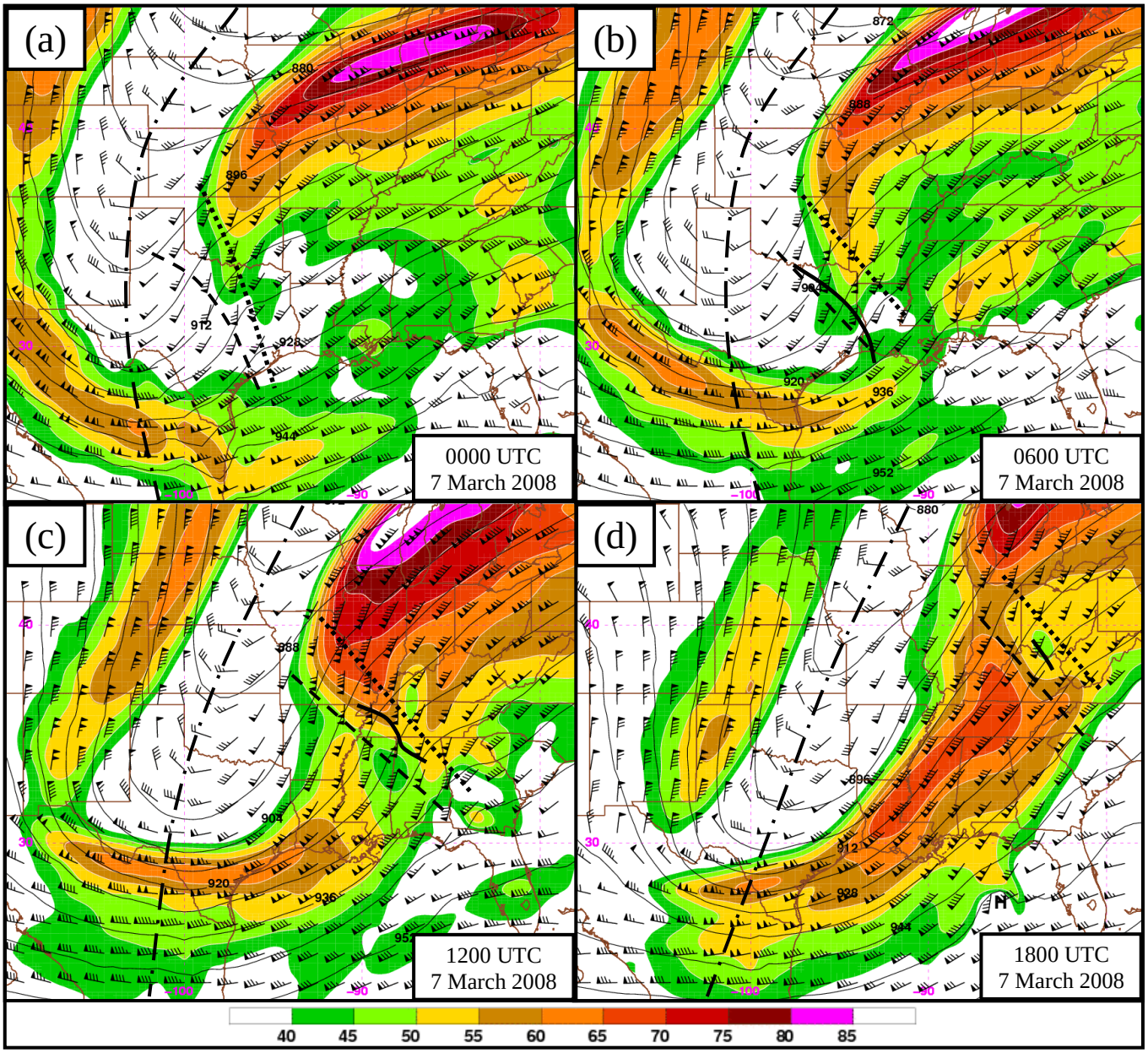

FIG. 6. 300-hPa height (thin solid; dam), wind (pennant, full barb, and half barb denote 25, 5, and 2.5 m s^{-1}, respectively), and wind magnitude (shaded according to the color bar; m s^{-1}) for 0000 (a), 0600 (b), 1200 (c), and 1800 (d) UTC 7 March 2008. Heavy solid lines denote approximate locations of IGW at 0600, 1200, and 1800 UTC 7 March 2008. Long dash–dotted, dashed, and dotted lines denote trough, inflection, and ridge axes, respectively. Generated from half-degree NCEP–GFS analysis data.

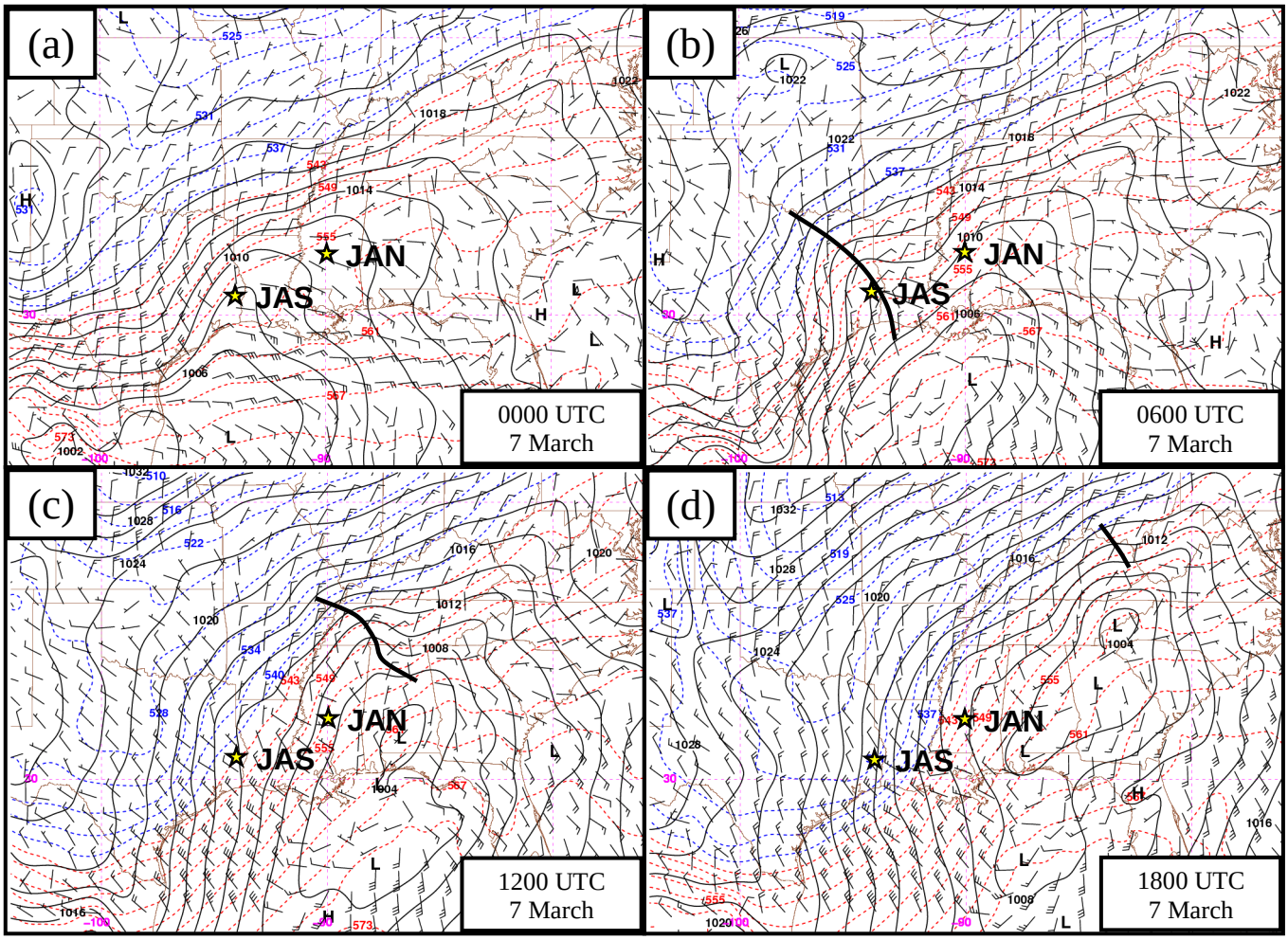

FIG. 7. Sea level pressure (SLP; thin solid; hPa), 1000–500-hPa thickness (blue dashed for ≤540 dam, red dashed for >540 dam), and 10-m wind (plotted according to the format of Fig. 6), at 0000 (a), 0600 (b), 1200 (c), and 1800 (d) UTC 7 March 2008. Locations of Jasper (JAS), TX and Jackson Thompson Field (JAN), MS are indicated. Heavy solid lines denote approximate locations of IGW at 0600, 1200, and 1800 UTC 7 March 2008. Generated from 20-km NCEP–RUC analysis data.

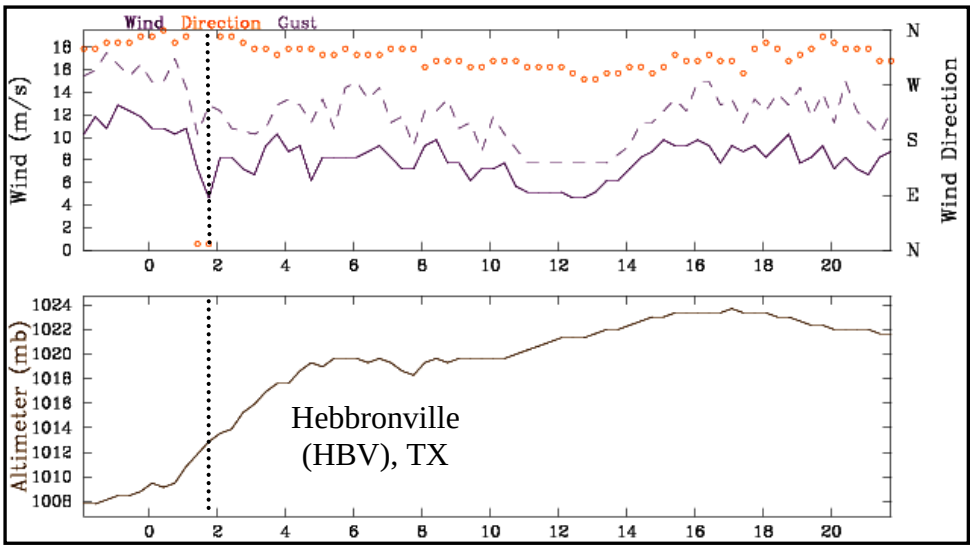

FIG. 8. Meteogram for Hebbronville (HBV), TX for the 24-h period ending at 2200 UTC 7 March 2008. Horizontal axes represent time in the format (*H*)*H*00 UTC. Top graph shows sustained wind (solid line; left axis; m s^{-1}), wind gust (dashed line; left axis; m s^{-1}), and wind direction (orange circles; right axis; cardinal). Bottom graph shows altimeter (hPa). Dotted lines denote estimated time of wave-passage. Generated from the University of Utah MesoWest Data Web Site (http://www.met.utah.edu/mesowest/).

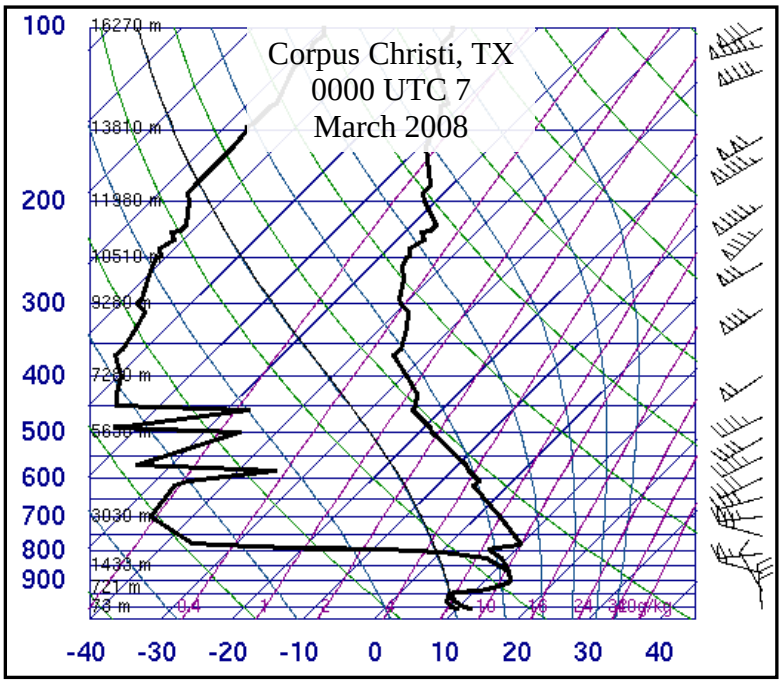

FIG. 9. Sounding in skew *T*–log*p* format for Corpus Christi (CRP), TX at 0000 UTC 7 March 2008. Winds plotted according to the format of Fig. 6. From the University of Wyoming Atmospheric Soundings Web Site (http://weather.uwyo.edu/upperair/sounding.html).

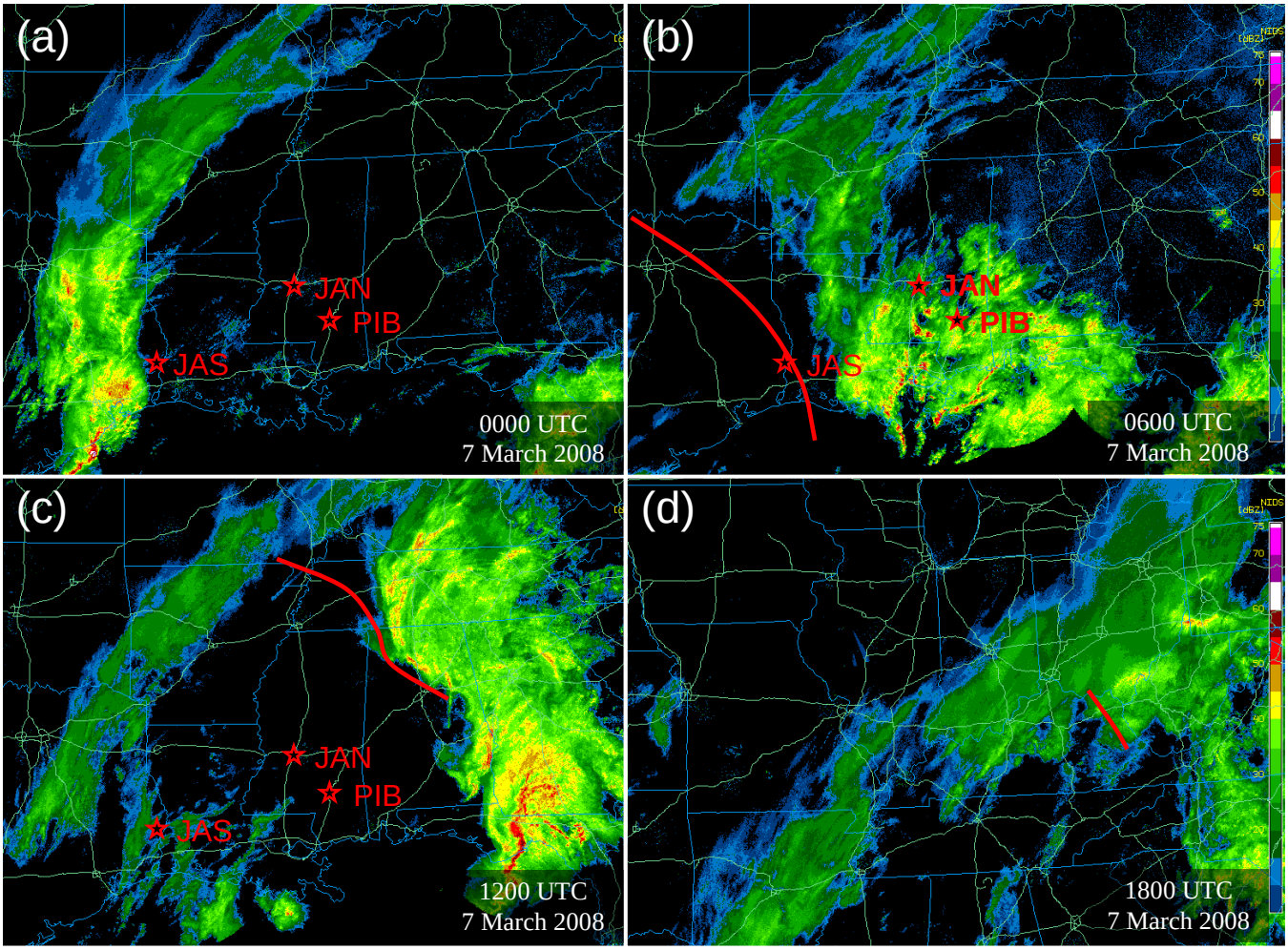

FIG. 10. As in Fig. 2 except for the southern (a, b, and c) and northern Mississippi Valley (d) at 0000 (a), 0600 (b), 1200 (c), and 1800 (d) UTC 7 March 2008. Locations of JAS, JAN, and Hattiesburg-Laurel Regional Airport (PIB), MS are indicated. Solid lines denote approximate locations of IGW at 0600, 1200, and 1800 UTC 7 March 2008.

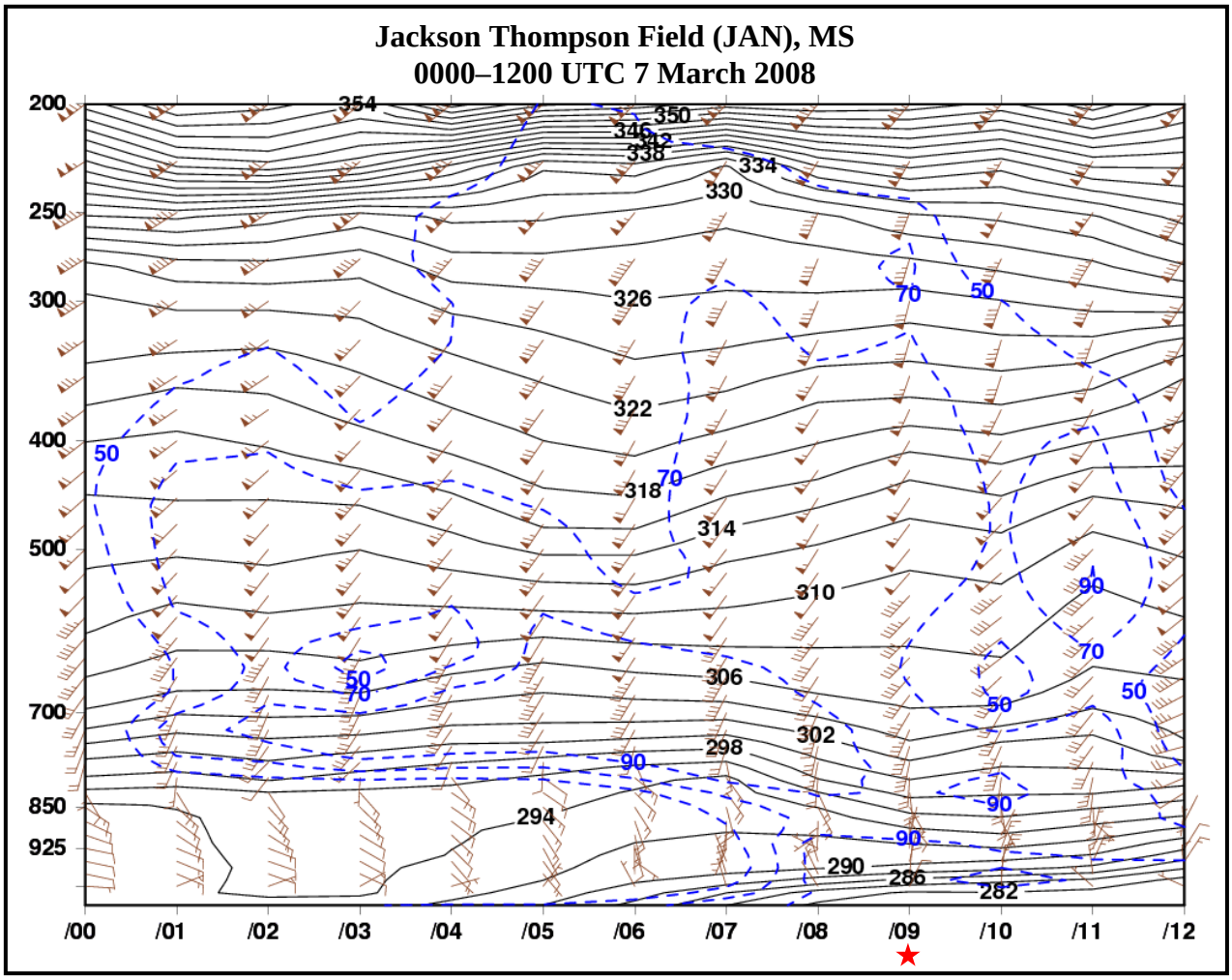

FIG. 11. Vertical time section for JAN from 0000–1200 UTC 7 March 2008 showing potential temperature (solid; K), relative humidity (dashed; %), and wind (plotted according to the format of Fig. 6) versus pressure (left axis; log*p*; hPa) and time (bottom axis; /*HH*00 UTC 7 March 2008). Star denotes approximate time of IGW passage. Generated from 20-km NCEP–RUC analysis data.

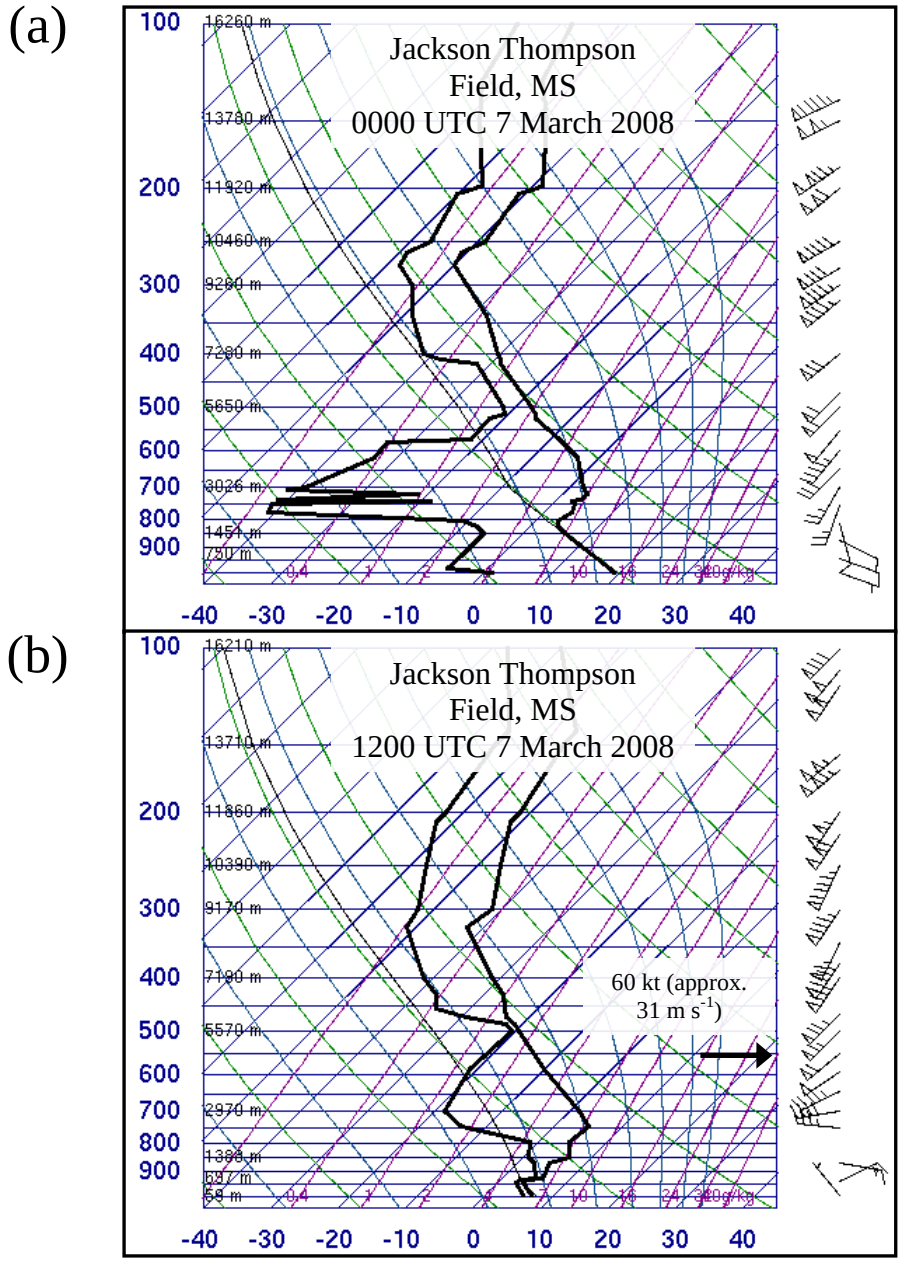

FIG. 12. As in Fig. 9 except for JAN at 0000 (a) and 1200 (b) UTC 7 March 2008. Heavy arrow denotes likely critical level (CL).

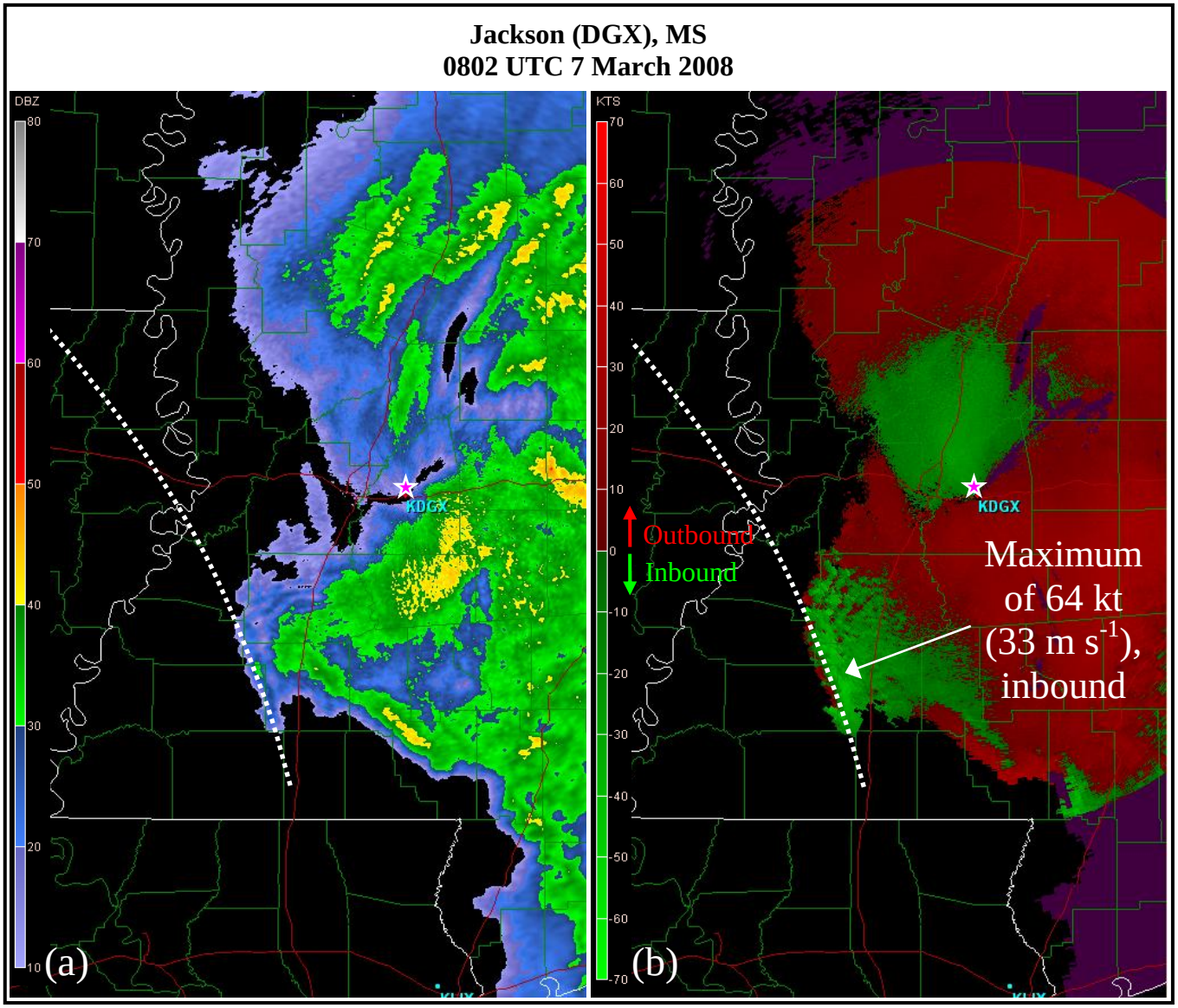

FIG. 13. WSR-88D base reflectivity (a; according to the color bar; dBZ) and velocity (b; according to the color bar; kt) for Jackson (DGX; station location indicated), MS at 0802 UTC 7 March 2008. Dotted lines denote approximate locations of IGW. Inbound and outbound velocities are indicated. Noted maximum inbound velocities denote likely CL. Generated using GR2Analyst and Level II WSR–88D data collected from the National Climatic Data Center Radar Resources Web Site (http://www.ncdc.noaa.gov/oa/radar/radarresources.html).

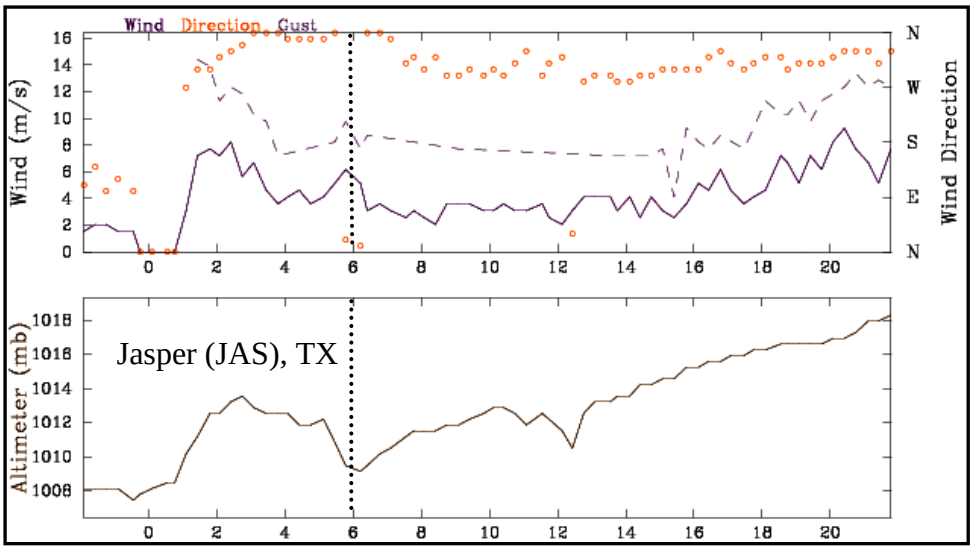

FIG. 14. As in Fig. 8 except for JAS.

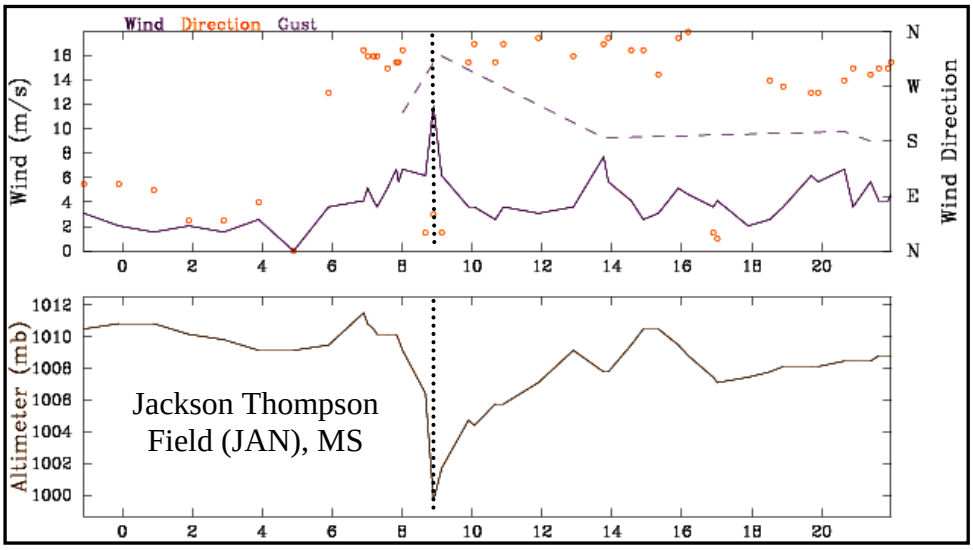

FIG. 15. As in Fig. 8 except for JAN.

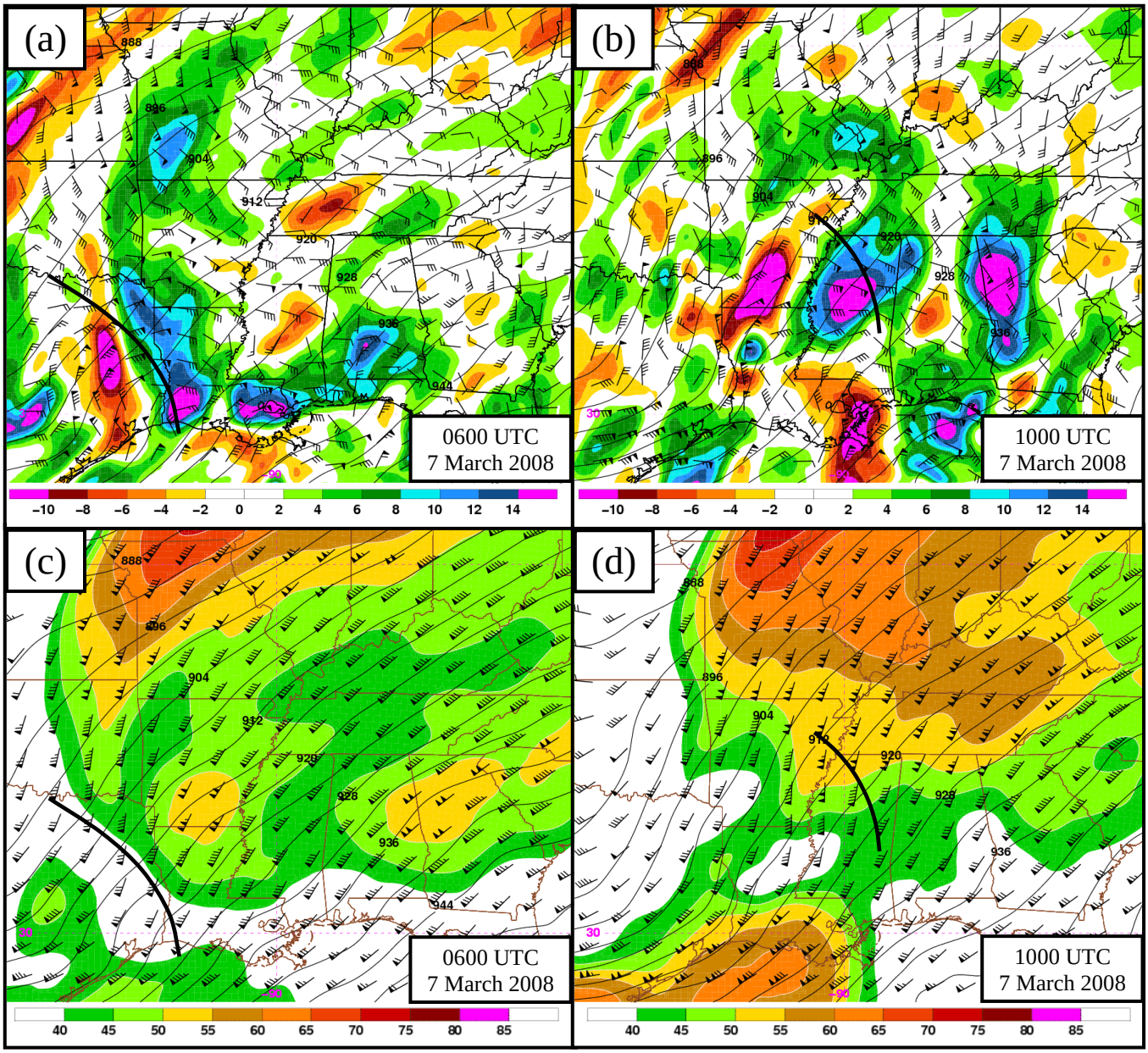

FIG. 16. Top row (a and b): 300-hPa height (thin solid; dam), ageostrophic wind (plotted according to the format of Fig. 6), and divergence (shaded according to the color bar; $\times 10^{-5}$ s^{-1}) for 0600 (a) and 1000 (b) UTC 7 March 2008. Bottom row (c and d): as in the top row except 300-hPa height (thin solid; dam), total wind (plotted according to the format of Fig. 6), and wind magnitude (shaded according to the color bar; m s^{-1}). Heavy solid lines denote approximate locations of IGW at 0600 and 1000 UTC 7 March 2008. Generated from 20-km NCEP–RUC analysis data.

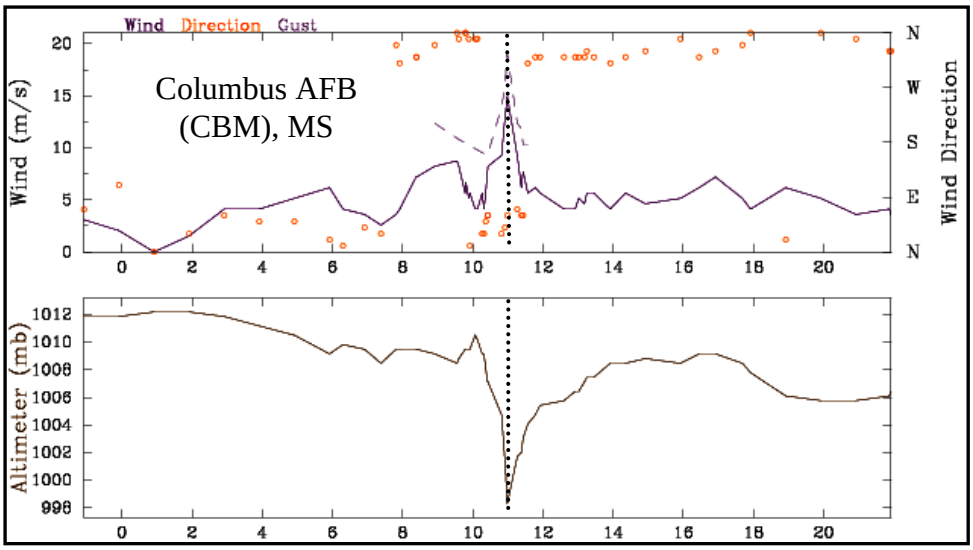

FIG. 17. As in Fig. 8 except for Columbus Air Force Base (CBM), MS.

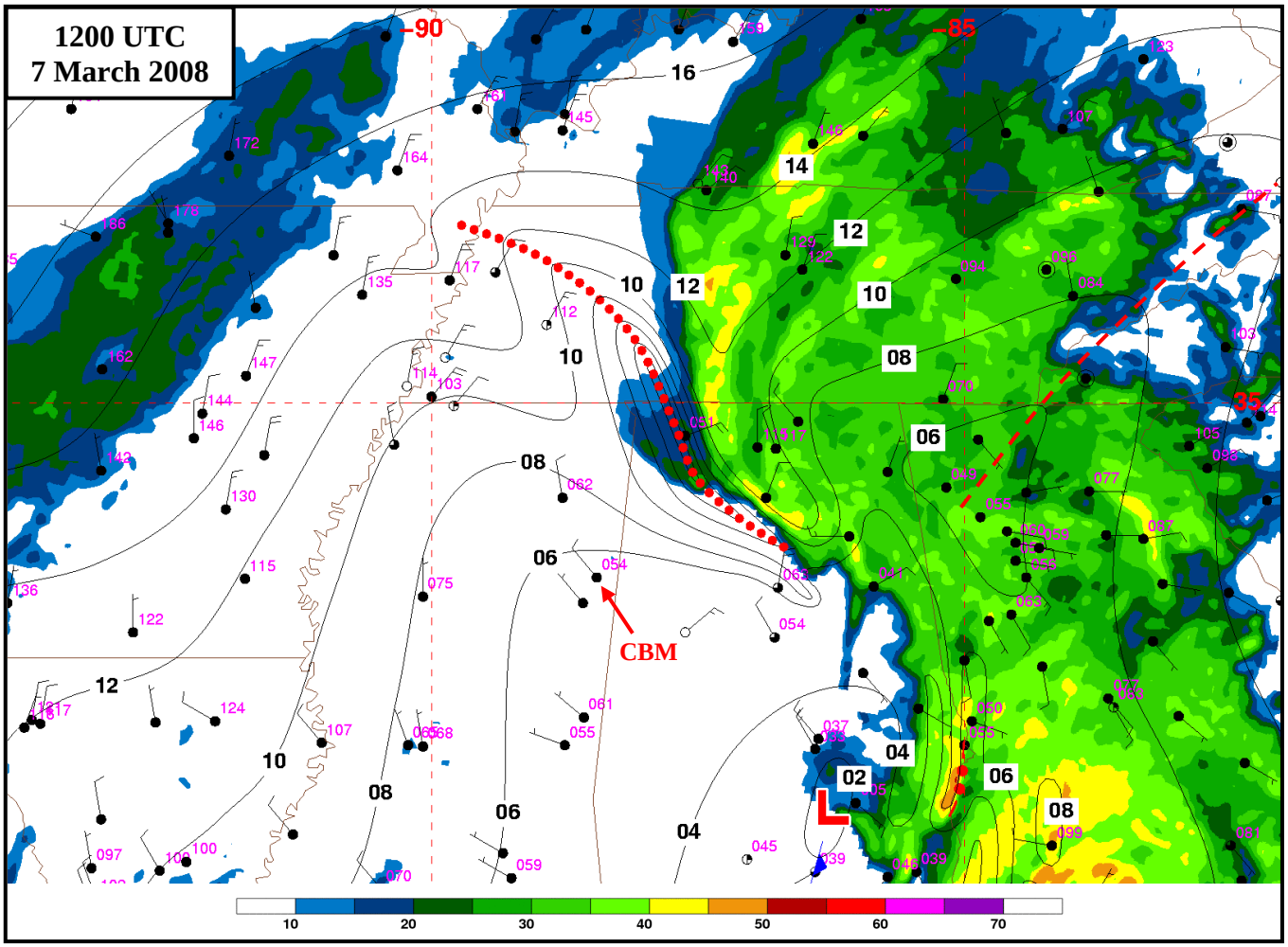

FIG. 18. Manually-generated surface analysis and composite WSR-88D base reflectivity (shaded according to the color bar; dBZ) for 1200 UTC 7 March 2008. SLP is contoured in the format 10*PP*.0 hPa. Weather stations [sky cover, SLP, and wind (plotted according to format of Fig. 6)] are plotted according to conventional notation. Dotted, dashed, and long dash–double dotted lines denote locations of IGW, secondary trough, and squall line, respectively. Location of CBM is indicated. Generated using NMAP2, a comprehensive product generator and part of the General Meteorology Package (GEMPAK) software, and surface observations from the University of Utah MesoWest Data Web Site (http://www.met.utah.edu/mesowest/).

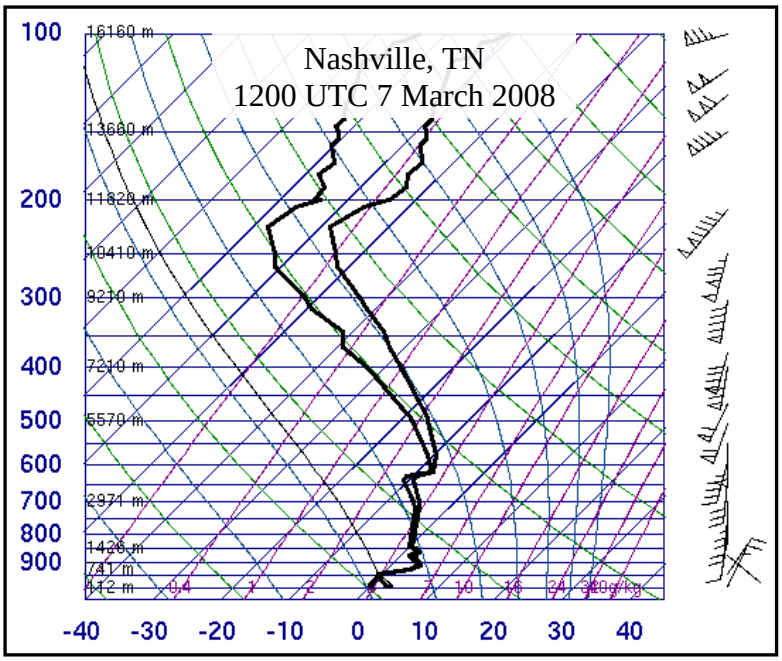

FIG. 19. As in Fig. 9 except for Nashville (BNA), TN at 1200 UTC 7 March 2008.

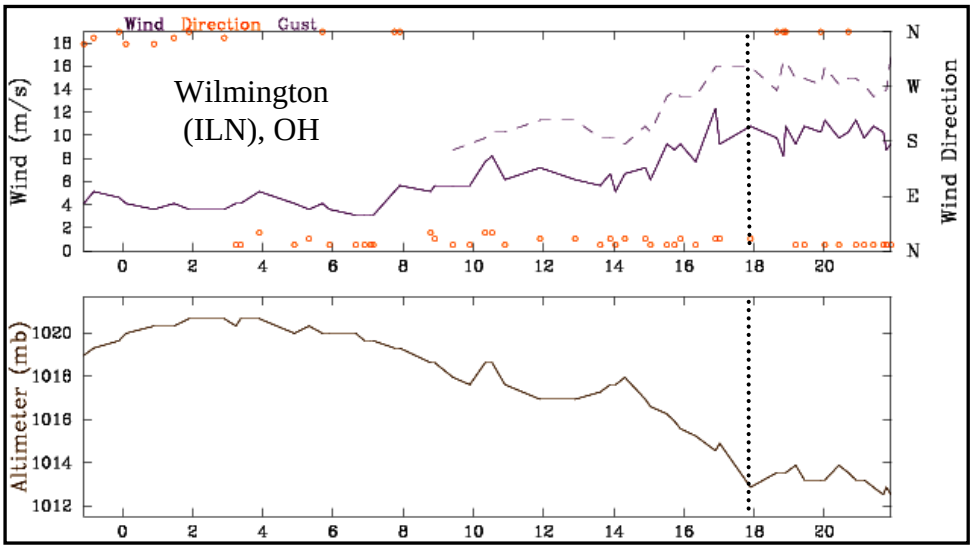

FIG. 20. As in Fig. 8 except for Wilmington (ILN), OH.

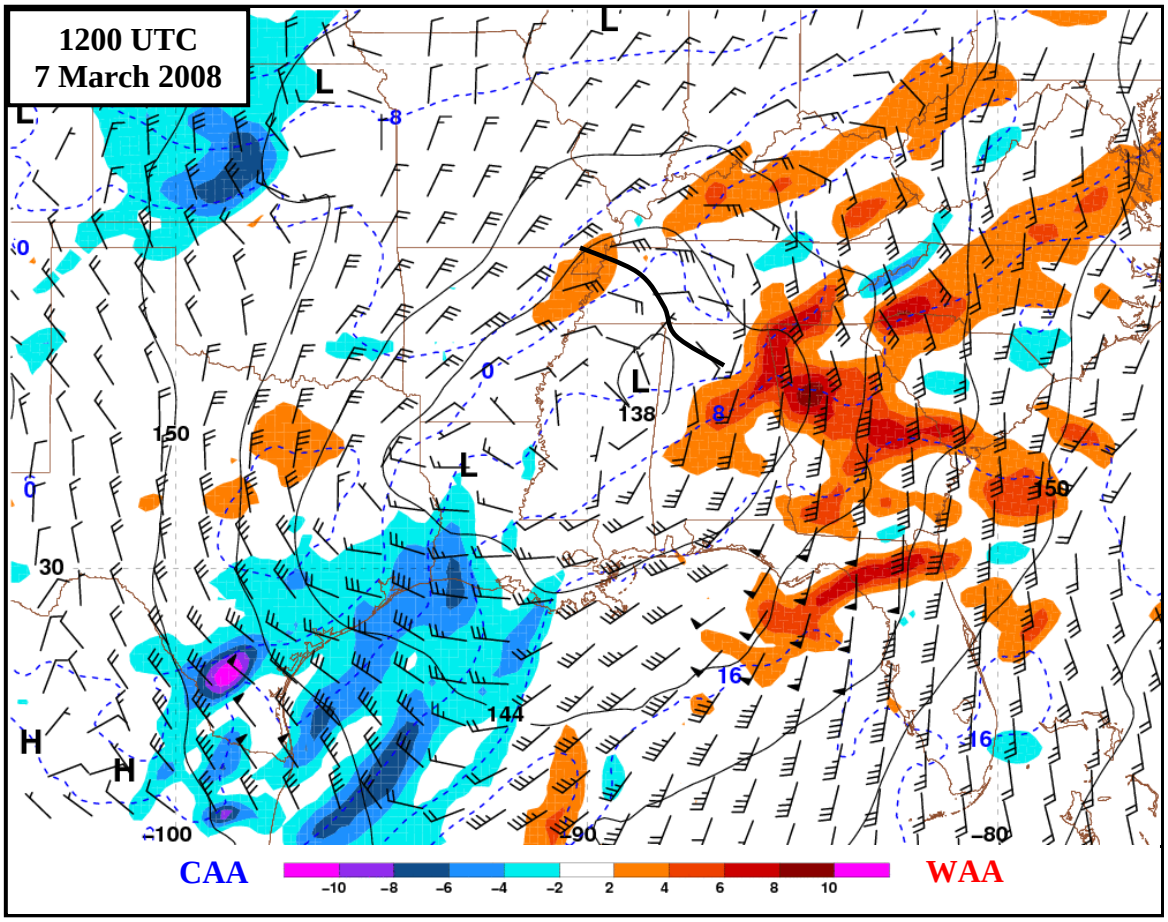

FIG. 21. 850-hPa height (thin solid; dam), wind (plotted according to the format of Fig. 6), temperature (dashed; °C), and thermal advection (shaded according to the color bar; $\times 10^{-4}$ K s^{-1}) at 1200 UTC 7 March 2008. Negative and positive thermal advection is denoted as CAA (cold air advection) and WAA (warm air advection), respectively. Heavy solid line denotes approximate location of IGW. Generated from 20-km NCEP–RUC analysis data.